Soil Dynamics and Earthquake Engineering 173 (2023) 108130

Contents lists available at ScienceDirect

Soil Dynamics and Earthquake Engineering

journal homepage: www.elsevier.com/locate/soildyn

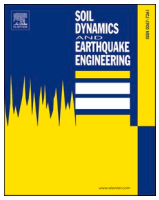

Experimental qualification of seismic strengthening of URM buildings in Nepal

Hammed O. Aminulai [a], Marco Baiguera [a], Duncan A. Crump [a], Anastasios Sextos [b], Mohammad M. Kashani [a,*]

[a] Faculty of Engineering and Physical Sciences, University of Southampton, UK
[b] Civil Engineering Department, University of Bristol, UK

ARTICLE INFO

Keywords:
URM buildings
Seismic retrofit
Splints and bandages
Seismic performance

ABSTRACT

Nepalese buildings are typically constructed using unreinforced masonry (URM) as the lateral load-bearing system. In the 2015 Nepal Gorkha earthquake several URM buildings suffered heavy damage. The limited economic resources available in the country and the challenge of strengthening a large portfolio of buildings highlight the need for low-cost retrofitting techniques. This paper presents a large-scale experimental campaign aimed at quantifying the seismic performance of a typical URM wall when strengthened with splints and bandages. This represents one of the retrofit techniques that are most widely-used in Nepal. A 5 × 3 m URM wall was constructed using 1:6 cement–sand mortar as per the mechanical properties identified by material testing in Nepal. The URM wall was tested under a two-way ramp cyclic loading. Typical crack patterns associated with URM were observed. The wall was subsequently retrofitted with 8 mm rebars as splints and bandages and tested to failure. The results show that the strength of the retrofitted wall is almost twice that of the URM wall. The observed crack damage improved from EMS-98 Grade 2, with horizontal and diagonal shear cracks in the mortar bed, to Grade 1, with hairline cracks on the rendered splints and bandages. Overall, the experiment demonstrated the efficiency of this practical, low-cost retrofitting technique that is tailored to traditional Nepalese URM buildings. This work can be used to advise local stakeholders in the construction industry as well as to act as a benchmark to improve the reliability of fragility functions for URM buildings in Nepal.

Author Statement

Hammed O. Aminulai: Writing the paper, conducting the experimental testing and data analysis.

Marco Baiguera: Postdoctoral researcher helping in conducting the experimental tests and writing the paper.

Duncan A. Crump: Experimental officer supporting the first author in conducting the experimental testing.

Anastasios Sextos: Editing the paper and co-supervising the PhD student (first author) and postdoctoral researcher (second Author).

Mohammad M. Kashani: lead supervisor, leading the research, supervising the student and postdoctoral researcher, and editing the paper.

1. Introduction

One of the main challenges for seismic regions in less-developed countries is related to the poor quality of construction that leads to disproportional damage and significant economic and life losses [1,2]. This was evidenced in India (Gujarat earthquakes, 2001), Iran (Bam Earthquake, 2003), Indonesia (Indian Ocean earthquake and Tsunami, 2004), Pakistan (Kashmir earthquake, 2005), China (Sichuan earthquake, 2008), Haiti (Haiti earthquakes 2010 and 2021), Peru (Peru earthquake, 2007) [3], Nepal (Gorkha earthquake, 2015) [4] and Mexico (2017) [5]. Notably, extensive damage to specific structural typologies, particularly masonry buildings, is also common in medium to high-income countries as well, see instance New Zealand (Christchurch, 2011), Japan (Tohoku earthquake and Tsunami, 2011) [6], Italy (Emilia earthquake, 2012) [7], and the extensive failure in Turkey and Greece after the Aegean Sea earthquake, 2020 [8].

Nepal is a characteristic case where high seismicity is associated with high structural vulnerability of the building portfolio, thus leading to substantial seismic risk [9]. The 7.8Mw Gorkha earthquake in 2015 caused extensive structural damage in 31 out of the 75 districts in the country, especially the Western and Eastern provinces, including the

* Corresponding author.
E-mail address: mehdi.kashani@soton.ac.uk (M.M. Kashani).

https://doi.org/10.1016/j.soildyn.2023.108130
Received 15 February 2023; Received in revised form 21 June 2023; Accepted 11 July 2023
Available online 22 July 2023

Fig. 1. Observed in-plane failure in piers and spandrels of an URM building [10].

Kathmandu Valley [10]. The mainshock and aftershocks of this earthquake caused 9000 casualties, with over 22,000 injuries, resulting in substantial damage to about 9500 school buildings [11,12]. The majority of buildings in rural areas were unreinforced masonry (URM) structures [13], which were deficient and poorly constructed with low quality, poorly prepared mortars, and even dry, and mud mortar mixes in some cases. They have no seismic detailing, hence little ability to sustain successive cycles of earthquake-induced lateral forces [14–18], a fact that overshadows some positive features such as durability and thermal insulation, which are vital in mountainous regions affected by the harsh climate and heavy monsoon rains [19].

The main problem, however, is that URM structures, being primarily designed to resist gravity loads, have low ductility and redundancy due to the lack of connections between the floor system and the walls, resulting in out-of-plane failure and collapse [20]. In addition, in-plane failure (Fig. 1) is also very common in the form of diagonal shear cracks in piers and spandrels, primarily along the mortar bed joints [10,21,22].

Several different methods have been developed and experimentally verified in the past to improve the strength and ductility of URM buildings [23–26]. Base isolation [27–31] and seismic damper techniques [32–35] have been used to reduce the effect of earthquake forces on URM structures. However, the first technique is expensive and can not typically be used for tall buildings and old structures [24,33], while the latter is mainly implemented to rehabilitate moment-resisting structures as it naturally requires large deformations to be activated, which is not feasible in rigid masonry systems [24]. Alternative methods include surface treatment with shotcrete and ferrocement [32,34–39], external steel reinforcement [24,40–44], post-tensioning with pre-stressed reinforcement [41,45–47], passive control systems [48], mesh reinforcement with conventional [49–54] or Aramid and Glass Fibre Reinforced Polymers (FRPs) [55–57], reticulation systems [58–61], and more recently the use of timber based system [62,63]. Such methods are effective in significantly improving the strength of existing masonry walls, but they are expensive and require high technical expertise required for implementation. This may result to be prohibitive for upgrading a large portfolios of buildings, especially in less developed regions [24], such as the Kathmandu region in Nepal.

This paper presents the results of a full-scale experimental investigation of the seismic response of URM walls under increasing cyclic loading, with the following aims:

(a) To verify the effectiveness of the splints and bandages retrofit technique, which is the standard method for upgrading URM buildings in Nepal [64]. This is done with the support of the Nepalese National Society for Earthquake Technology (NSET);
(b) To quantity the improvement in seismic performance of the wall in terms of strength and ductility;
(c) To lay the foundations for a database of experimental data and facilitate the calibration of high-order numerical models, enhancing the accuracy of existing fragility curves and inform seismic assessment and retrofit guidelines in Nepal and more in generale in south-central Asia.
(d) To outline a series of practical recommendations for efficiently implementing the studied retrofit scheme for the local professional community.

The experimental tests presented in this paper were performed as a part of the Seismic Safety and Resilience of Schools in Nepal (SAFER) project [EP/P028926/1, www.safernepal.net], which aims to contribute to all aspects of seismic resilience in the region, e.g., from new models for seismic hazard to novel micromechanical modelling of mortar joints and brick-mortar interfaces in masonry structures [65], through fragility assessment of school buildings in the Kathmandu valley in Nepal [13,66,67], large-scale experimental campaigns to qualify existing walls retrofitted with low-cost wire steel mesh [4] and new methods for low-cost seismic isolation systems [68].

2. Overview of the experimental programme

2.1. Experimental design

The experimental campaign was carried out in the Large Structures Testing Laboratory (LSTL) at the National Infrastructure Laboratory (NIL) of the University of Southampton. Tests were conducted on a 5 × 3 m full-scale masonry brick wall, which is representative of typical one-storey school buildings in Nepal. The wall specimen was constructed based on the recommendations made by the National Society for Earthquake Technology - Nepal (NSET) [64]. Fig. 2 (i and ii) show the schematic representation of the geometry of the wall specimen, which is made of clay bricks set in 15 mm thick 1:6 cement-sand mortar using the British bond as recommended in Ref. [64] and the Nepalese building code (NBC 203, 2015) [69]. The material properties are in line with previous bespoke tests conducted in Nepal for the determination of the

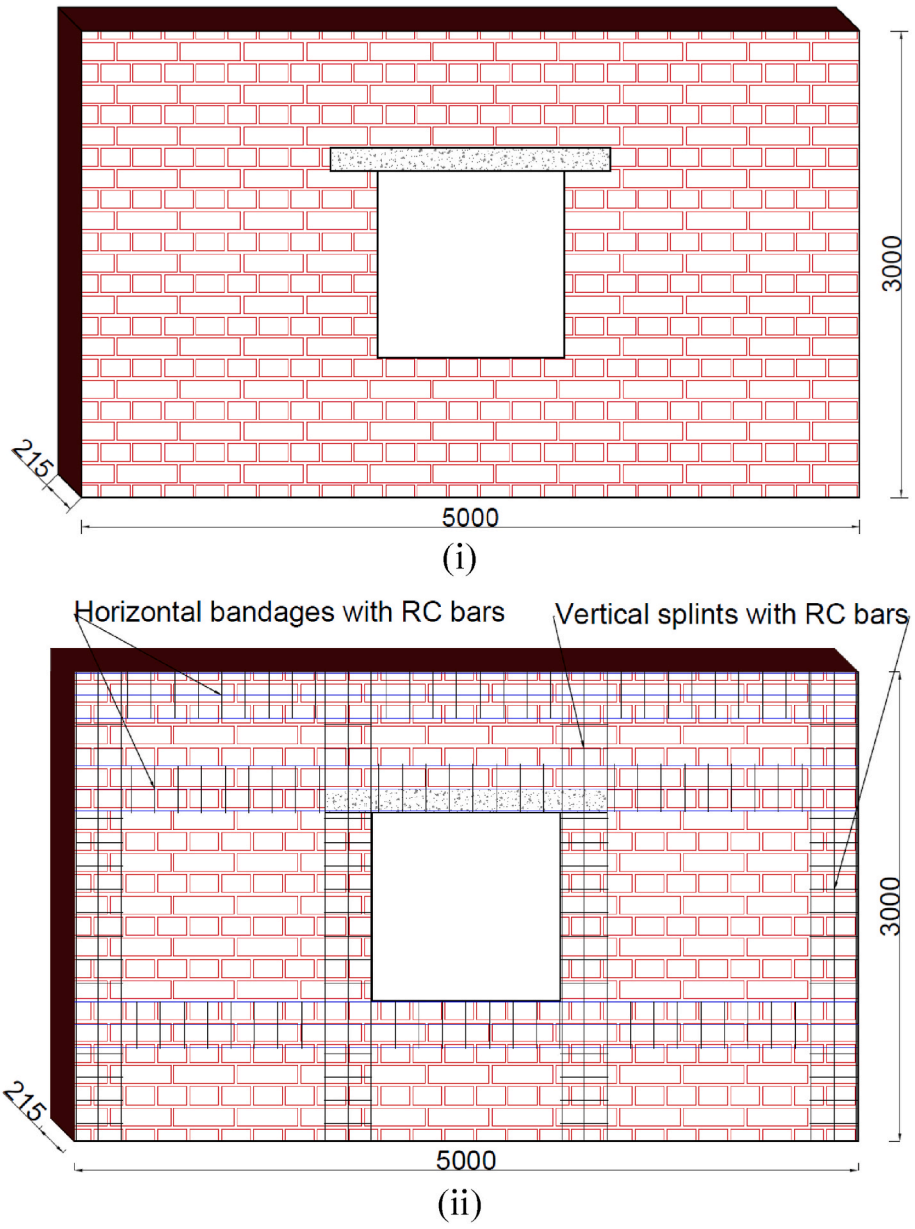

Fig. 2. Schematic diagrams of the masonry wall: (i) unreinforced; (ii) reinforced with splint and bandages (dimensions in mm).

Fig. 3. The retrofitted wall: (a) rebar splint and bandages; (b) overview after covering with layers of mortar screed.

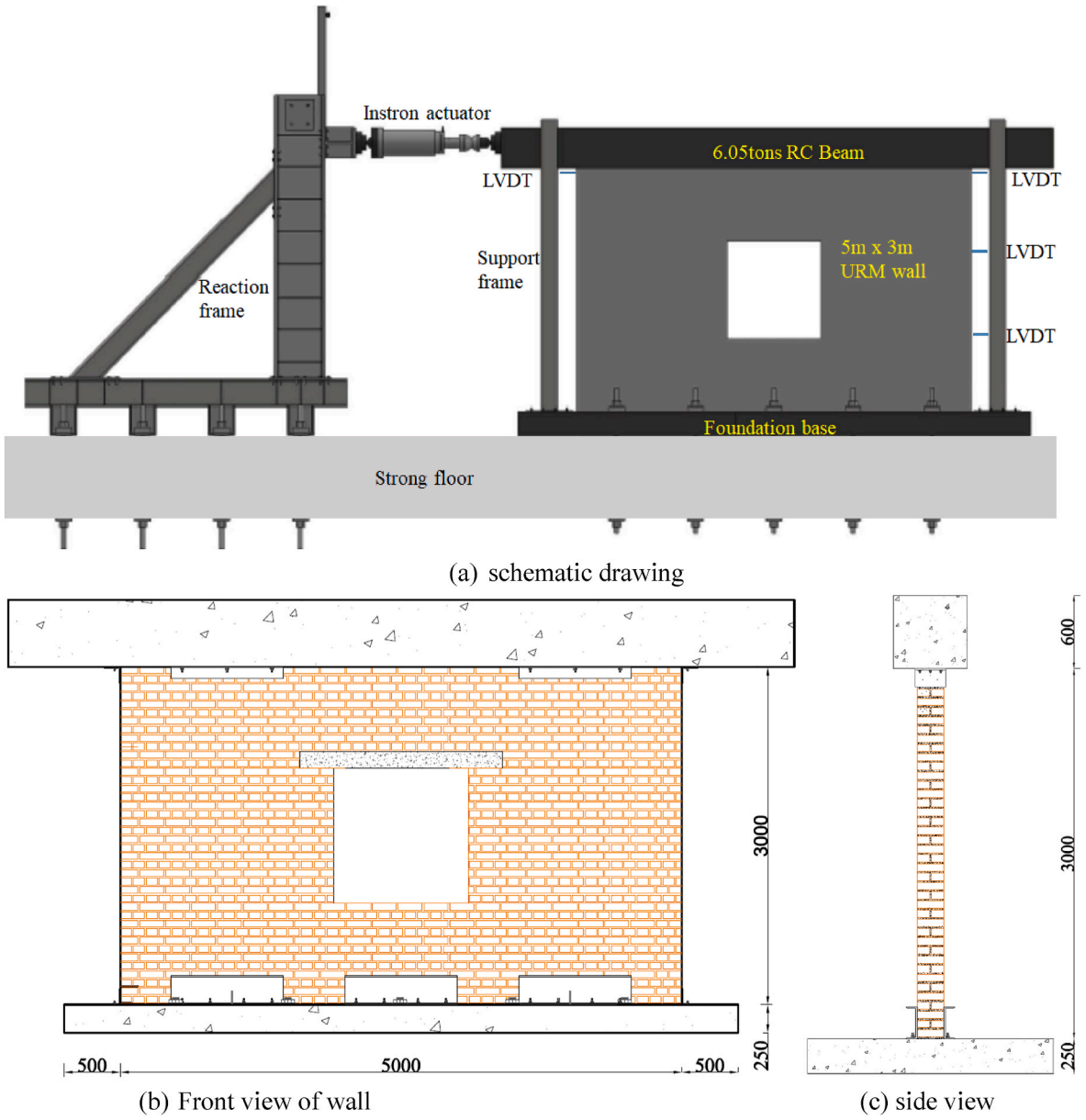

Fig. 4. The experimental test setup.

mechanical properties of the materials used to ensure consistency with the local construction practice. The URM wall (Fig. 2(i)) was built following the standard construction practice in Nepal, without any seismic detailing. The retrofitting technique consists of splints and bandages (Fig. 2(ii)). The wall is confined at the base with parallel flange channels (PFC) sections and angle irons fixed at the wall's sides and end to prevent sliding and ensure only in-plane movement of the masonry wall during testing.

The URM wall is subjected to two-way ramp cyclic loading to induce the usual shear cracking pattern and failure associated with URM structures [70–72]. Next, the wall is retrofitted on both sides with splints and bandages (Fig. 2(ii)) made with 8 mm reinforcement bars anchored at the top of the wall and the foundation slab for seismic strengthening.

The bent ends of the splints (about 150 mm) are anchored at the top of the URM through 20 mm diameter holes filled with high-strength resins (HIT-HY 170 injection mortar) and fixed in 12 mm diameter 200 mm deep holes at the base with high strength grout (SikaGrout 3200) (Fig. 3(a)). The bandages are wrapped around the wall and tied together. These are also connected to the splints at the points where they cross each other (top of the wall, sill and lintel). The connected splints and bandages are fixed to the wall with 8 mm anchorage rods set with epoxy resins in 10 mm holes drilled into the bricks, and they are covered with the low-strength 1:6 cement-sand mortar screed to an average thickness of 65 mm in three layers (Fig. 3(b)).

2.2. Experimental setup

A hydraulically powered 250 kN Instron hydropuls linear actuator with ±125 mm stroke was used to apply a two-way ramp cyclic lateral load [55,72–74] to the end of a 6.05tons RC beam attached to the top of the masonry wall (Fig. 4). The RC beam weight is equivalent to the estimated load of the roof for a typical floor wall. The actuator is also connected to a data acquisition system (Strainsmart 8000) to record the load and displacement from the actuator during testing. The wall is confined at both the base with parallel flange channels (PFC) sections and the top with equal angle sections to avoid any sliding and ensure the

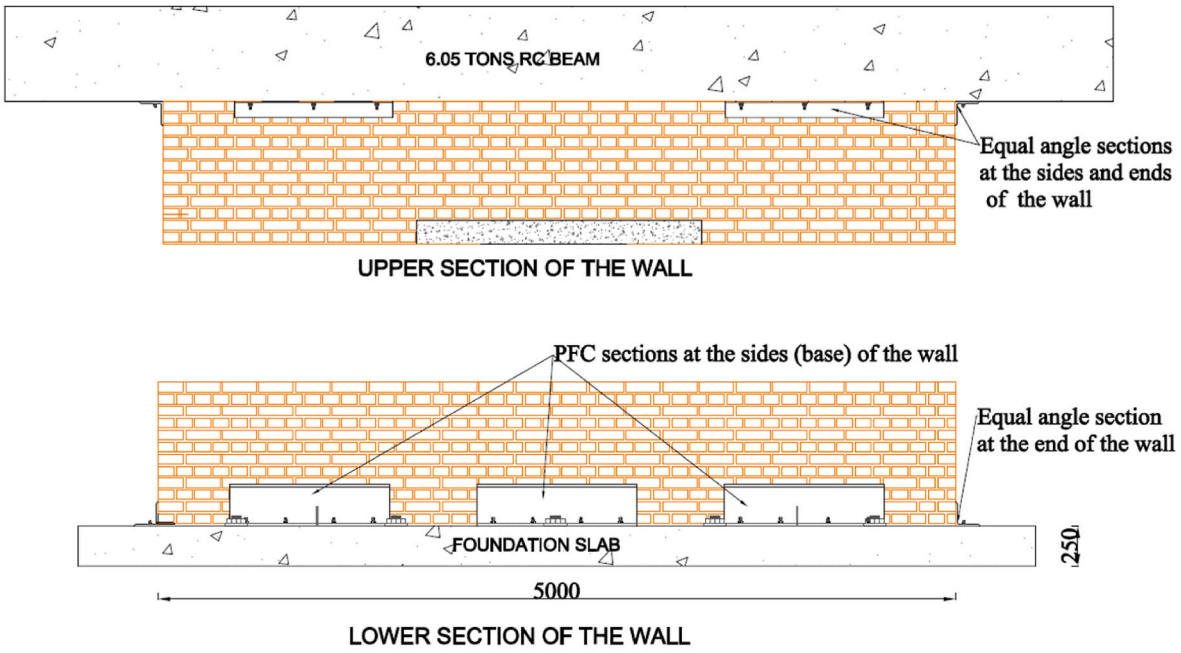

(d) views of equal angles and PFC sections connections to wall (front and back)

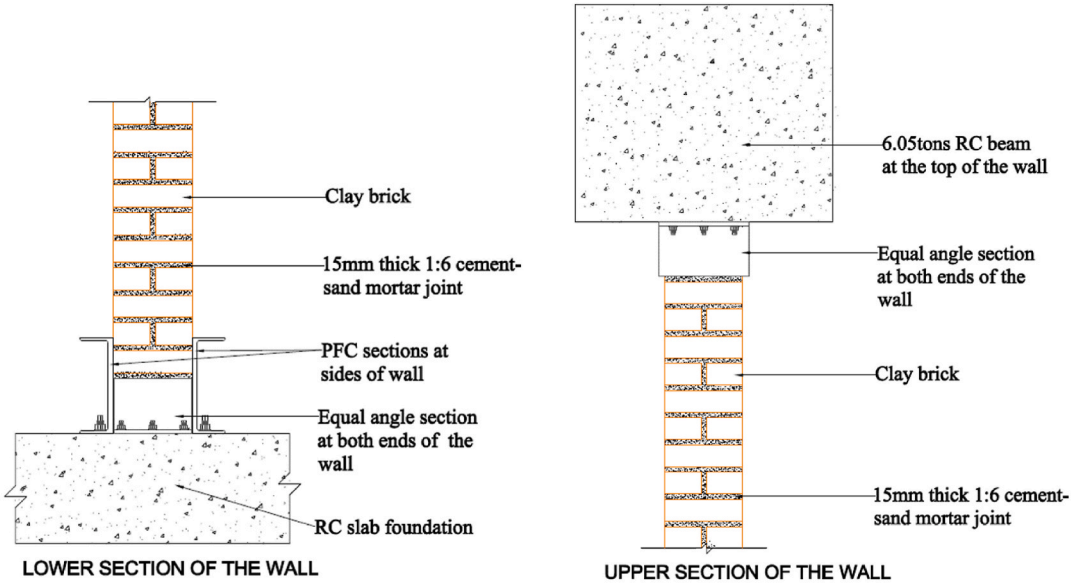

(e) Side views of wall with the angles and PFC connections

Fig. 4. (*continued*).

wall deforms in the direction of the applied displacement load only. The Instron actuator is controlled by the MTS Aeropro system in terms the input parameters (loading protocol, safety limits, and stop criteria).

2.3. Instrumentation and loading protocol

The test instrumentation involves four Linear Variable Differential Transformers (LVDTs) with 50 mm stroke for measuring lateral displacements (position) connected to the wall and a multichannel data acquisition unit (Strainsmart 8000). Three LVDTs are connected to the wall's right end at 1 m interval from the top, while the fourth is fixed at the loading end of the wall.

The wall was painted white with black dots marked at 300 mm centres to measure the displacement field using the Digital Image Correlation (DIC) technique (Fig. 4(b)) using LaVision's Davis Imaging Software (Davis 10.0.5 [75]) involving two cameras (Imager E-Lite 5 M) fitted with Nikon AF Nikkor 28 mm f/2.8D (28 mm focal length and 2.8 maximum aperture) and 50 mm f/1.8D (50 mm focal length and 1.8 maximum aperture) lenses. The first camera with the 28 mm f/2.8D captures the images on the wall, while the second camera focuses on a wall section close to the window edge.

The load was applied using displacement control as a two-way ramp cyclic loading (Fig. 5) by gradually increasing the amplitude of the displacements, utilising a 1 mm/min frequency for each cycle. The loading on the URM specimen continued until the shear and lateral cracks, introduced mainly at the brick-mortar interface, were observed at 3 mm and 4 mm amplitudes. Then, the retrofitted wall was loaded with the same protocol, the difference being that the loading was increased to 6 mm amplitude as no damage was observed at the end of the 4 mm loading sequence.

(f) Laboratory implementation

Fig. 4. (*continued*).

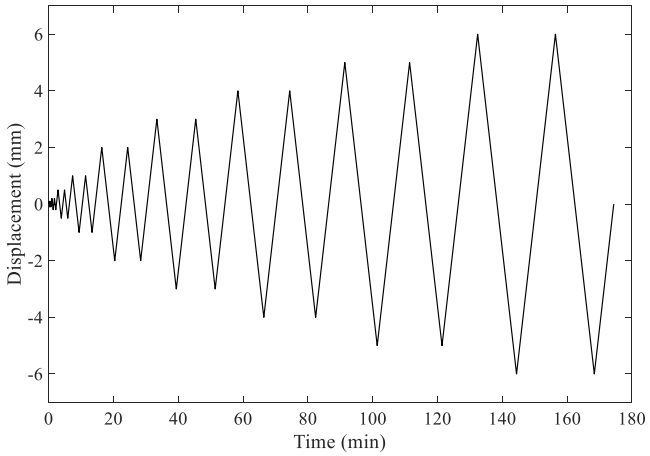

Fig. 5. The experimental loading sequence.

3. Experimental results and discussion

3.1. Material characterisation

The materials used in the experimental test were selected such that the mechanical properties match the typical construction materials in Nepal as provided by the local partners in Nepal (NSET-Nepal). These material properties were determined from the tests conducted on materials in Nepal as part of the SAFER project mandate. The selected materials were subjected to laboratory tests per the relevant material testing standard to ascertain the materials' conformity and suitability to replicate the Nepali construction materials. The clay bricks (six pieces) with nominal dimensions of 215 × 100 × 60 mm were tested for conformity, density, and compressive strength following BS EN 771–1:2011+A1:2015 [76] and BS EN 772–1:2011+A1:2015 [77]. Fig. 6 (i) shows the stress-strain behaviour of the clay bricks, while the mean density and compressive strength are summarised in Table 1.

The cement mortar and render used for the wall have a 1:6 cement-to-sand ratio with an average thickness of 15 mm and 65 mm, respectively. The compressive strength and density of the render and mortar were determined using 100 mm cube samples following the guidelines in BS EN 1015–11:2019 [78] and BS EN 1015–10:1999 [79], respectively (Table 1). The masonry and rendering mortars are classified as M2.5 and CSII based on their compressive strength values. Fig. 6(ii) and 6(iii) show the stress-strain behaviour of the mortar and render. Fig. 6 (ii) shows the compressive strength of the mortar used during the wall construction. As the wall was constructed in two stages, the mortar samples were collected at each stage, with the average values presented in Table 1.

Tensile tests were carried out on samples of the retrofitting rebars to assess their mechanical properties. The tensile test was performed at the Testing Structures and Research Laboratory (TSRL) of the University of Southampton Boldrewood Campus, using the Instron 8032 test machine with 100 kN capacity and ±50 mm stroke to determine the mechanical properties of the bars. It involves subjecting the rebars to different loading rates before and after the yielding of the bars as specified in BS EN ISO 6892–1:2019 [81]. At the same time, a dynamic extensometer measures the corresponding strain. The summary of the test result on 3 bars is presented in Table 1. The mechanical test on the rebars indicates that it is a B500C steel bar as the yield (549 MPa) and ultimate (644Mpa) strength falls within the specified minimum and maximum values of BS 4449:2005+A3:2016 [80]. Also, the strength ratio of 1.17 is within the allowable range ($\geq 1.15, < 1.35$) [80].

3.2. Seismic performance of unreinforced masonry walls

3.2.1. Progression of damage and crack pattern

The applied cyclic, in-plane lateral displacement loading resulted in extensive cracking of the URM wall. During the first part of the test, crack initiation and growth were monitored by visual inspection (after each load cycle) and video imaging. No crack was observed at lower levels of amplitude until 3 mm, when lateral crack damage was observed near the base of the wall (Fig. 7(i) and (ii)). At increasing amplitudes, diagonal cracks were observed at 4 mm amplitude at the top of the window opening extending towards the upper part of the URM (Fig. 7 (iii) and (iv)).

. As shown in Fig. 8(i-iv), there is no noticeable crack damage at the 1 mm loading cycle (Fig. 8(i)), while the 2 mm loading cycle image shows the beginning of the crack at the lower part of the wall (Fig. 8(ii)). The horizontal crack in Fig. 8(ii) becomes more pronounced and visible at the 3 mm loading with other cracks that were not noticeable by visual inspection (Fig. 8(iii)). Further, the 4 mm loading cycle image captures

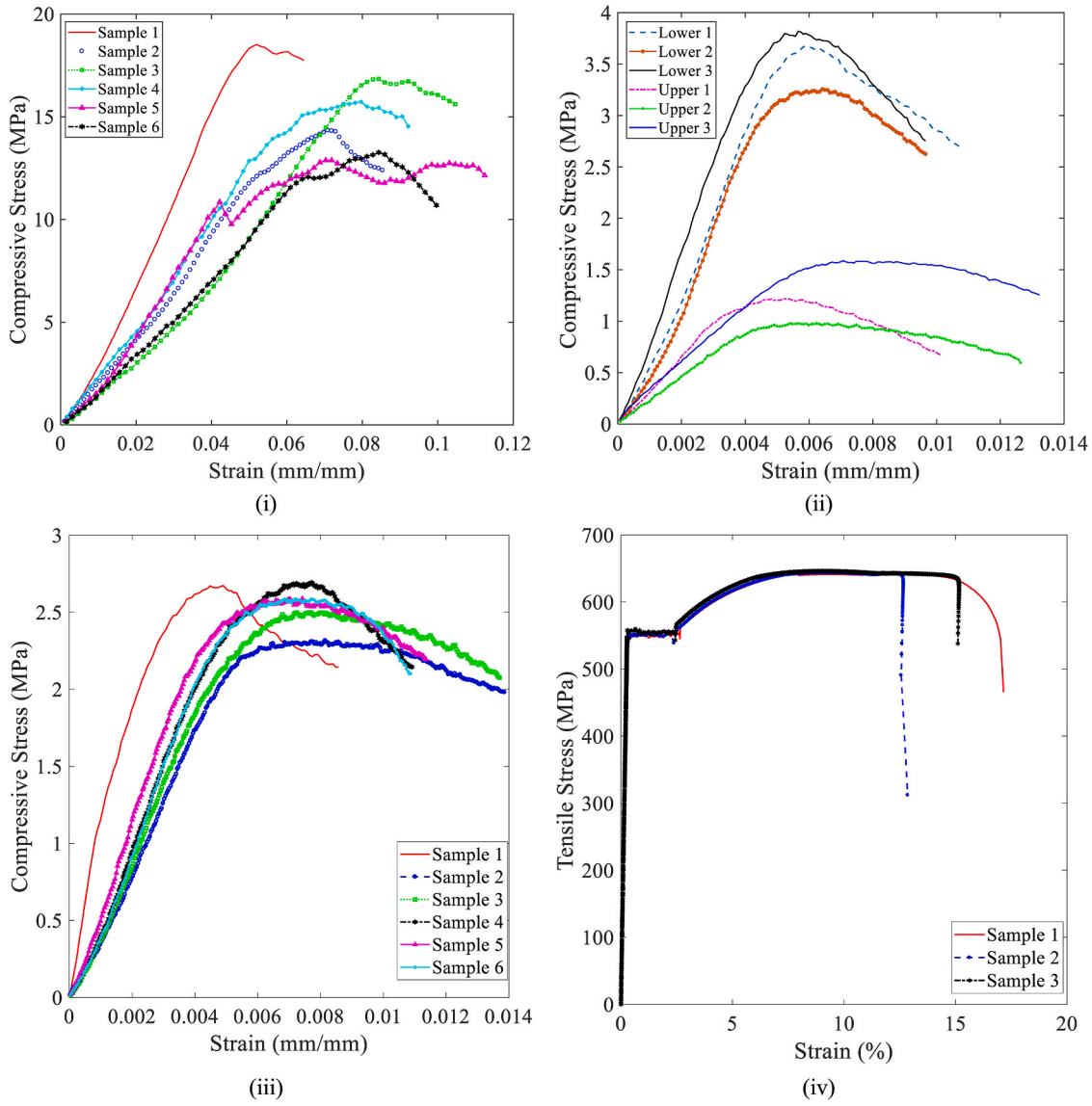

Fig. 6. Typical stress-strain behaviour of the wall component materials; (i) clay brick, (ii) wall mortar, (iii) wall render and (iv) 8 mm reinforcement bars.

Table 1
Masonry wall material properties.

Material	Parameter	On site values (Nepal)	Average Values (Experiment)	No of Specimens	Standard
Bricks	Dimensions (L × B × H)	230 × 100 × 63.5	215 × 100 × 60	6	[76]
	Compressive strength (MPa)	5.97	15.28	6	[77]
	Young's modulus (MPa)		253.49	6	[77]
	Density (Kg/m^3)	1384.80	2116.3	6	[77]
Mortar	Dimensions (L × B × H)	100 × 100 × 100	100 × 100 × 100	6	
	Compressive strength (MPa)	3.87	2.43 (M2.5)	6	[78]
	Young's modulus(MPa)		551.75	6	[78]
	Density, (Kg/m^3)	1830	1575.4	6	[79]
Render	Dimensions (L × B × H)		100 × 100 × 100	6	
	Compressive strength (MPa)		2.57 (CS II)	6	[78]
	Young's modulus(MPa)		751.53	6	[78]
	Density (Kg/m^3)		1592.8	6	[79]
8 mm (B500) Rebar	Young's modulus (MPa)		197,500	3	[80]
	Yield strength, f_y (Mpa)	415	549	3	[80]
	Ultimate strength, f_u (Mpa)		644	3	[80]
	Yield strain, ε_y		0.00278	3	[80]
	Ultimate strain, ε_u		0.07392	3	[80]
	Strain ratio ($\varepsilon_u/\varepsilon_y$)		26.59	3	[80]
	Strength ratio, (f_u/f_y)		1.17	3	[80]

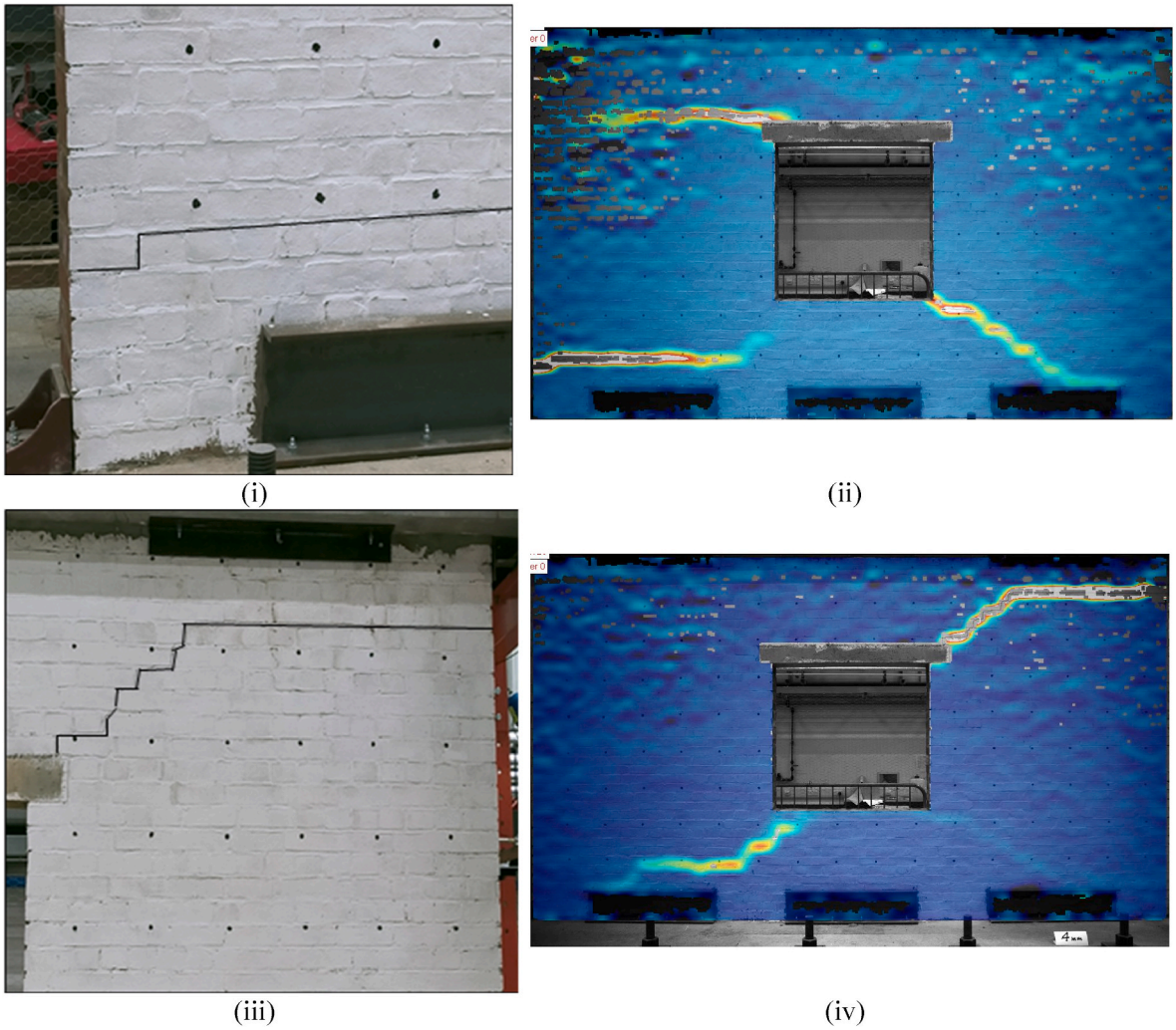

Fig. 7. Failure modes of URM at different levels of displacement loading: (i) Lateral crack at the base at 3 mm; (ii) Digital Image Correlation corresponding to 3 mm amplitude; (iii) diagonal cracks at the edge of window opening towards the top at 4 mm (iii) DIC image corresponding to 4 mm amplitude.

all the observed crack damage at the 3 mm loading and the diagonal crack damage at the edges of the window opening resulting from the 4 mm loading cycle (Fig. 8(iv)). The processed DIC images further revealed minor crack mechanisms that could not be observed by visual inspection during testing, such as the diagonal crack at the bottom-left of the window opening (Fig. 7 (iv)) and the crack at the top-left of the opening (Fig. 7(ii)).

All cracks were observed to initiate and develop in the mortar joints of the URM wall and are classified as the typical shear failure of masonry walls [72,82]. According to the European Macroseismic Scale (EMS-98) [83], this type of failure falls under the moderate damage Grade 2 class and represents the typical damage of a masonry building during a moderate earthquake.

3.2.2. Lateral force-displacement response

The force-displacement behaviour and the corresponding DIC of the URM wall at each loading cycle are shown in Fig. 8 (i – iv). The ultimate load-carrying capacity of the URM wall increased with the displacement loading from the 1 mm amplitude (49.9 kN) and 2 mm amplitude (95.80 kN) until about 3 mm displacement loading when the lateral crack at the lower part of the wall occurred, leading to a slight reduction in the loading capacity (95.62 kN). This crack further reduces the wall's stiffness by about 34.7%, hence its load-carrying capacity. Further reduction in the load-carrying capacity was observed at the 4 mm displacement loading (82.96 kN), where more significant diagonal crack damage occurred at the edge of the window towards the upper part of the URM wall.

3.3. Seismic performance of the retrofitted masonry walls

3.3.1. Retrofitting method

The slightly damaged URM wall was then retrofitted with splints and bandages made with 8 mm high-yield rebars and covered with the 1:6 cement-sand mortar screed. The splints, which are vertical members, are fixed to the wall by anchoring the bent ends (150 mm long) of the bars in 20 mm holes drilled at the top of the wall (just below the RC beam) and filled with Hilti epoxy resins (HIT-HY 170 injection mortar). The lower ends are placed into 12 mm diameter 200 mm deep holes, drilled into the concrete base slab and sealed with high-strength grout (SikaGrout 3200). Finally, the splints, comprising three vertical bars spaced by 350 mm long bars (bent 50 mm at both ends to have a span of 250 mm), are placed at both ends of the wall and edges of the window opening, as shown in Fig. 3(a).

At the same time, the bandages comprising three horizontal bars along the spandrels are fixed to the top of the wall and the lintel and sill of the window opening. The bars' bent ends (150 mm long) are tied together at the ends of the wall to form closed rings. The splints and bandages are held close to the wall by anchor bars fixed in epoxy-filled holes drilled into the bricks at intervals. Finally, the splints and bandages are covered in three layers with the 1:6 cement-sand mortar

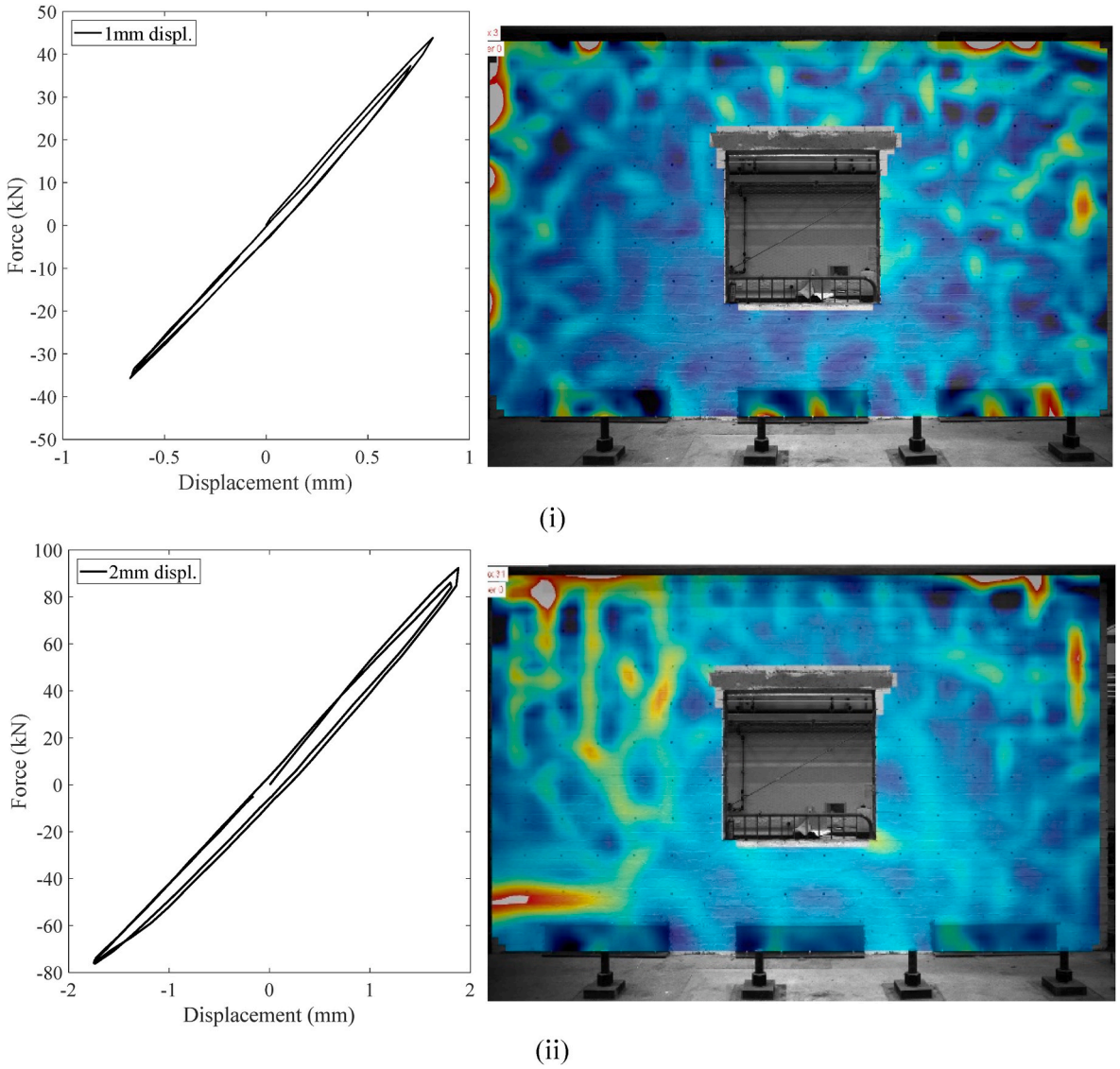

Fig. 8. The force-displacement curves and the corresponding DIC images at each loading cycle of the test on the URM wall: (i) 1 mm displacement apmitude (ii) 2 mm displacement apmitude (iii) 3 mm displacement apmitude (iv) 4 mm displacement apmitude.

screed to about 65 mm thickness.

The retrofitted wall was subjected to the same two-way ramp cyclic displacement loading protocol used on the URM wall. This loading was subsequently incremented to 6 mm amplitude (having observed little or no cracks on the wall) and finally pushed monotonically until a 20% drop in force (the test was stopped at this point for safety reasons). The wall was visually inspected for crack damage after each loading cycle. The retrofitted wall exhibited some little hairline cracks (red lines in Fig. 9) and spalling on the wall's rendered parts (mainly at the upper part below the RC beam), which increased as the test progressed and was more noticeable at the end of the monotonic push. There were also diagonal and horizontal cracks in the mortar joint at the lower part of the wall (green lines in Fig. 9). The observed cracks fall under the negligible to slight damage category (Grade 1) class of failure according to the European Macroseismic Scale (EMS-98) [83]. The Grade 1 failure refers to damages with slight non-structural damage having only hairline cracks and the fall of small pieces of plaster.

The processed DIC images of the retrofitted wall could not track the crack progression resulting from the wall displacement due to the spacing of the dot marks on the wall. For more precise processing of such tests in the future, the dots should be made closer and denser to each other.

3.3.2. *Lateral force-displacement response*

The force-displacement response of the retrofitted wall to the applied two-way ramp cyclic displacement loading is presented in Fig. 10. The plot includes the monotonic loading applied after the 6 mm cyclic loading and shows an increase in the ultimate load-carrying capacity of the retrofitted wall. The wall was pushed monotonically to about 183 kN, almost double the URM wall's load-carrying capacity (95.62 kN). In addition, the wall stiffness increased with the displacement loading amplitudes until the monotonic loading sequence, when the test was stopped for safety reasons.

3.3.3. *Comparison of the observed damages and force-displacement relationship of the URM and retrofitted wall*

The retrofitted wall exhibited a higher load-carrying capacity [42] and had a higher effective stiffness than the URM wall, as seen from the comparison in Table 2 and Fig. 11 below. The ultimate load-carrying capacity of the masonry wall increased from 95.8 kN to 182.97 kN,

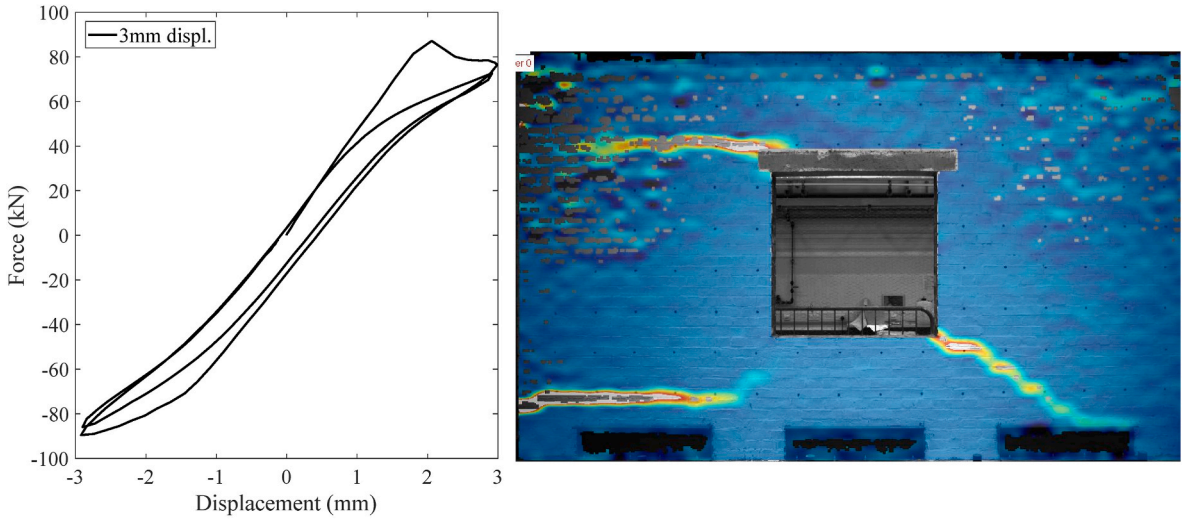

(iii)

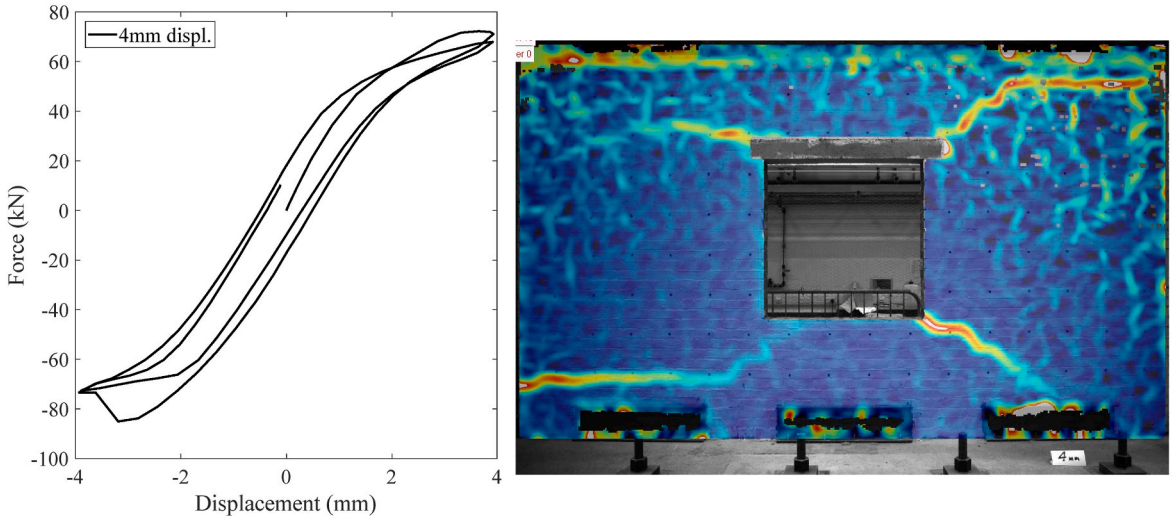

(iv)

Fig. 8. (*continued*).

indicating an approximately 91% increment. Also, the retrofitting reduces the crack damage failure (Grade 2) observed in the URM wall to just some hairline cracks (Grade 1) on the rendered splints and bandages band (Fig. 9) with little spalling of the rendering mortar at the top of the wall [83]. At 4 mm amplitude loading, the stiffness of the retrofitted wall to the URM wall increased by 92.4|%. This shows the effectiveness of the retrofitting method applied to the URM wall after the damage from the initial test.

The strength increasing (R_S) and deformation capacity increasing (R_D) ratios of the masonry wall are estimated using equations (1) and (2) proposed by Yamaguchi et al. (2016) [84].

$$\text{Strength ratio}, R_S = \frac{\sigma_r}{\sigma_{ur}} \tag{1}$$

where, σ_r is the maximum strength of the retrofitted wall and σ_{ur}, is the maximum strength of the URM wall. The average of the absolute value of the maximum strengths in the tension and compression direction is applied to equation (1) in the case of the cyclic loading test.

$$\text{Deformation capacity ratio}, R_D = \frac{D_r}{D_{ur}} \tag{2}$$

where D_r is the drift angle of the retrofitted wall at 80% of the maximum strength, and D_{ur}, is the drift angle of the URM wall. If the strength does not decrease to 80% of the maximum, the maximum drift angle given in the loading test is applied to equation (2).

The strength increasing ratio and deformation capacity ratio estimated from equations (1) and (2) are 1.91 and 7.72, respectively. These values show the strength increase by the retrofitted wall against the URM wall and its subsequent resistance to deformation.

The effective stiffness, K_e, defined as the secant stiffness, K_{sec}, is defined as the ratio between the lateral resistance and the corresponding wall displacement [73] expressed as the ratio of the maximum load at each loading cycle to its associated displacement (Fig. (12)). It was estimated from the expression below:

$$K_{sec} = \frac{\left|F^{+}_{max,i}\right| + \left|F^{-}_{max,i}\right|}{\left|\delta^{+}_{max,i}\right| + \left|\delta^{-}_{max,i}\right|} \tag{3}$$

where, K_{sec}, is the effective stiffness (kN/mm), $F^{+/-}_{max,i}$ is the peak force (kN) in the tension and compression loading direction for each loading cycle and $\delta^{+/-}_{max,i}$, is the maximum displacement (mm) in the tension and compression loading direction at each loading cycle.

Fig. 13(a) shows the normalised stiffness of the masonry wall to the

Fig. 9. Observed crack damage to the retrofitted wall at the end of the test.

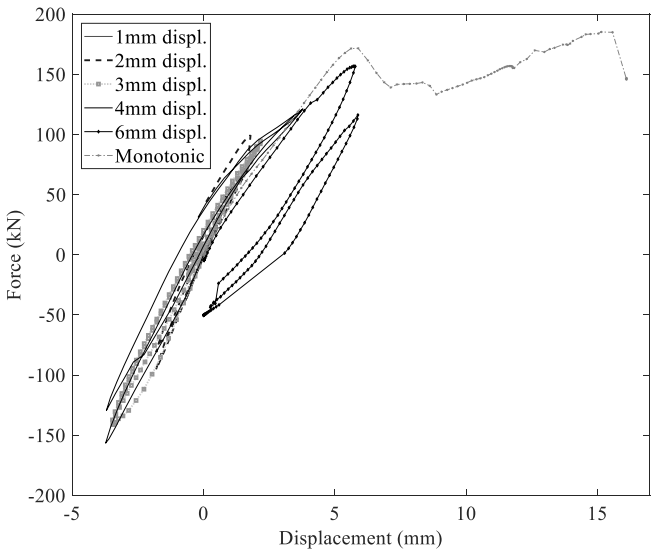

Fig. 10. Force-displacement response of the retrofitted wall.

Table 2
Maximum forces and observed damages during the test.

Cycle No.	Unreinforced Masonry wall (URM)		Reinforced Masonry wall (RM.)	
	Max. force (kN)	Observed damages	Max. force (kN)	Observed damages
1 mm	49.91	No crack	−38.42	No crack
2 mm	92.52	No crack	110.49	No crack
3 mm	95.62	Horizontal cracks at the lower part of the wall	−141.44	Hairline cracks on the rendering on the wall
4 mm	82.96	Diagonal cracks upward from the edge of the window opening	−156.72	Hairline cracks on the rendering on the wall
6 mm	–	–	156.85	Cracks in the mortar joints of the lower part of the wall
Monotonic	–	–	187.97	Shear failure of the bolts in the top angle plates.

corresponding displacement estimated from equation (1). The secant stiffness of the wall decreases as the displacement load increases with crack formation at each loading cycle. The retrofitted wall exhibited a higher stiffness resistance than the URM at each loading displacement. The percentage increase in the normalised stiffnesses between the retrofitted and URM walls are 8.1%, 26.4% and 32.2% for the 2 mm, 3 mm and 4 mm displacement loadings, respectively.

The energy dissipation capacity is an essential parameter in assessing the seismic behaviour of masonry structures. The amount of energy dissipated for each cycle of loading displacement amplitude was calculated as the area within the hysteretic loop (Fig. 12). Fig. 13(b) shows the cumulative energy dissipated by the masonry wall tested. The wall exhibited a similar trend in both the URM and the retrofitted wall, showing increasing energy dissipation capacity with increasing displacement loading. As expected, the retrofitted wall had a higher dissipation capacity than the URM wall though they both had similar energy dissipated at the 1 mm loading amplitude. The cumulative energy dissipated by the retrofitted wall increased from the URM wall by 4.3% (98.3kNmm to 102.5kNmm), 14.3% (125.9kNmm to 143.9kNmm) and 24.2% (144.1kNmm to 179kNmm) at the 2 mm, 3 mm and 4 mm displacement amplitude, respectively. The retrofitted wall further had a cumulative energy dissipated increment at the 6 mm loading of 210.3kNmm. The cumulative energy dissipated by the retrofitted wall at 6 mm results in a 46% increment in the energy dissipated by the URM at 4 mm. This increment is close to the 50% recommended by researchers [24,25,42,85–87]. The retrofitted wall has a higher energy dissipation due to the splint and bandages preventing the propagation of shear crack damage along the mortar bed joints of the wall.

The equivalent viscous damping is a good indicator of the energy dissipation capacity and the stability of the hysteresis behaviour [88]. It is computed as the ratio between the energy dissipation of the completed cycle and its corresponding force-displacement response (elastic energy)

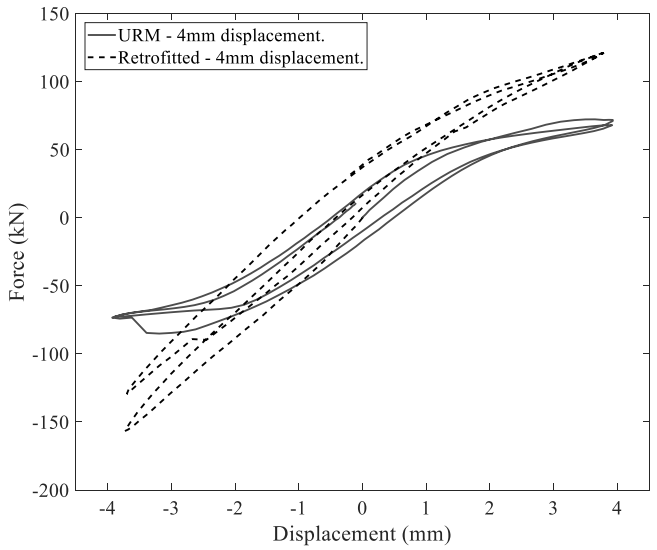

Fig. 11. Force–displacement comparison of both URM and retrofitted walls at 4 mm displacement loading.

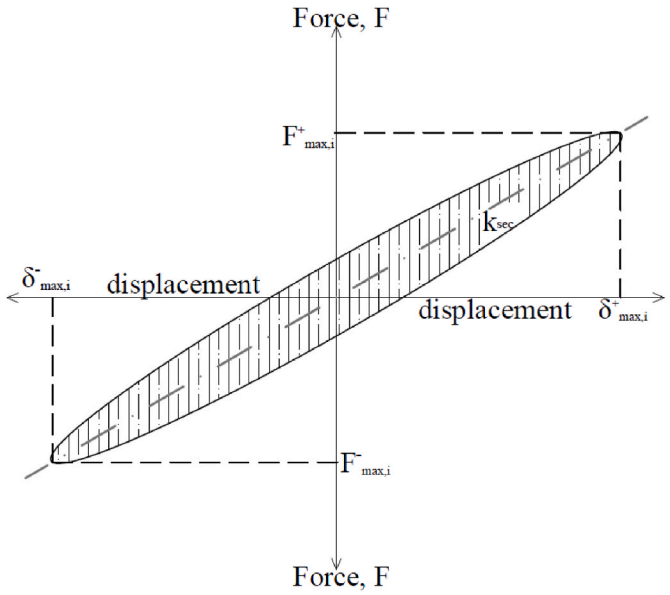

Fig. 12. Typical hysteretic response of masonry structure.

(Fig. 12). It is calculated for each loading cycle (Equation (4)).

$$\xi_i = \frac{1}{2\pi} \frac{W_i}{F_i^+ \delta_i^+ + F_i^- \delta_i^-} \tag{4}$$

where, W_i is the energy dissipated at each loading cycle (kN.mm), $F_i^{+/-}$ is the peak force in the tension and compression loading direction for each loading cycle (kN) and $\delta_i^{+/-}$, is the maximum displacement at each loading cycle in both the tension and compression loading direction.

Fig. 13(c) shows the equivalent viscous damping of the masonry wall at the different loading amplitudes. The viscous damping decreases with increasing loading amplitude in the URM and retrofitted wall. For example, 83.8%, 93.7% and 96.5% decreased for the 2 mm, 3 mm and 4 mm, respectively, from the 1 mm loading amplitude in the URM wall. A similar trend is observed in the retrofitted wall, having reduced viscous damping by 84%, 93.6%, 95.8% and 95.9% for the 2 mm, 3 mm, 4 mm and 6 mm, respectively.

4. Practical guidelines for retrofitting unreinforced masonry walls in Nepal

The use of external steel reinforcement, especially the splints and bandages, significantly increases the stiffness by about 32% at 4 mm loading amplitude, ductility and in-plane strength (about 91%) capacity of the retrofitted wall [42,89]. Furthermore, the availability of steel reinforcement and the expertise needed for fixing helps to reduce the overall cost of the retrofitting technique to about one-third of the cost of reconstructing the wall [4].

From the experimental test carried out on the masonry wall using parameters provided by NSET-Nepal [64], the procedure for the retrofitting of Nepalese school buildings should be as follows.

- The clay bricks should be set in 1:6 cement-sand mortar as recommended by the NBC [69] rather than the mud mortar specified by NSET-Nepal.
- The splints, comprising three vertical bars spaced with 350 mm long bars (bent 50 mm at both ends such that it spans 250 mm) at 150 mm centres, are fixed at the edges of the walls' opening, ends and corners (Fig. 14(i) and (iii)). The spanning and locations of the splints and bandages are as recommended by NSET-Nepal [64].
- The top end of the splints should be bent (about two-thirds the width of the wall) and fixed in holes drilled at the top of the wall. Alternatively, the lower ends are fixed straight into holes in the foundation slab (Fig. 14(ii) and (iv)) instead of bent into the lower part of the wall.
- The bandages, comprising three horizontal bars spaced with bars similar to the splints, are placed at the top of the wall, the lintel level and the sill of the window. The bent ends of the bandages are tightened together to form a closed ring around the wall (Fig. 14(ii) and (iv)).
- The splints and bandages are held close to the wall by anchor bars made from reinforcement. The bars are bent at the ends, fixed into holes drilled (about half the width of the wall) into the bricks, and filled with epoxy resins at about 1 m centres (Fig. 14(v)). The anchor bars should be fixed with epoxy resin as it is stronger than the cement slurry recommended by NSET-Nepal.
- The splints and bandages are afterwards covered with a 1:6 sand-cement render/plaster mixture in layers, depending on the thickness. Sand-cement render/plaster should be used on the splint and bandages instead of the concrete recommended by NSET-Neapl, as it was found suitable for the wall and will be cheaper and faster to install.
- The retrofitting is done on both sides of the wall.

It is noted that the proposed guideline is limited to its application to URM walls that are constructed using the Nepalease construction technique. Further experimental testing and numerical parametric studies are needed on the other typologies recommended by NSET and the application of the technique on a full-scale URM building.

5. Conclusions

This paper presents a benchmark large-scale experimental testing under in-plane cyclic loading of a typical Nepalese school URM wall using the same construction technique and materials in Nepal. The experiment aimed to investigate the effectiveness of the splints and bandages technique proposed by NSET-Nepal, in improving the seismic performances of Nepalese school URM walls after moderate seismic activity. The findings of the experimental test resulted in the following conclusions.

1. The URM wall showed significant stiffness at the lower displacement load until the slight horizontal crack damage occurred at 3 mm

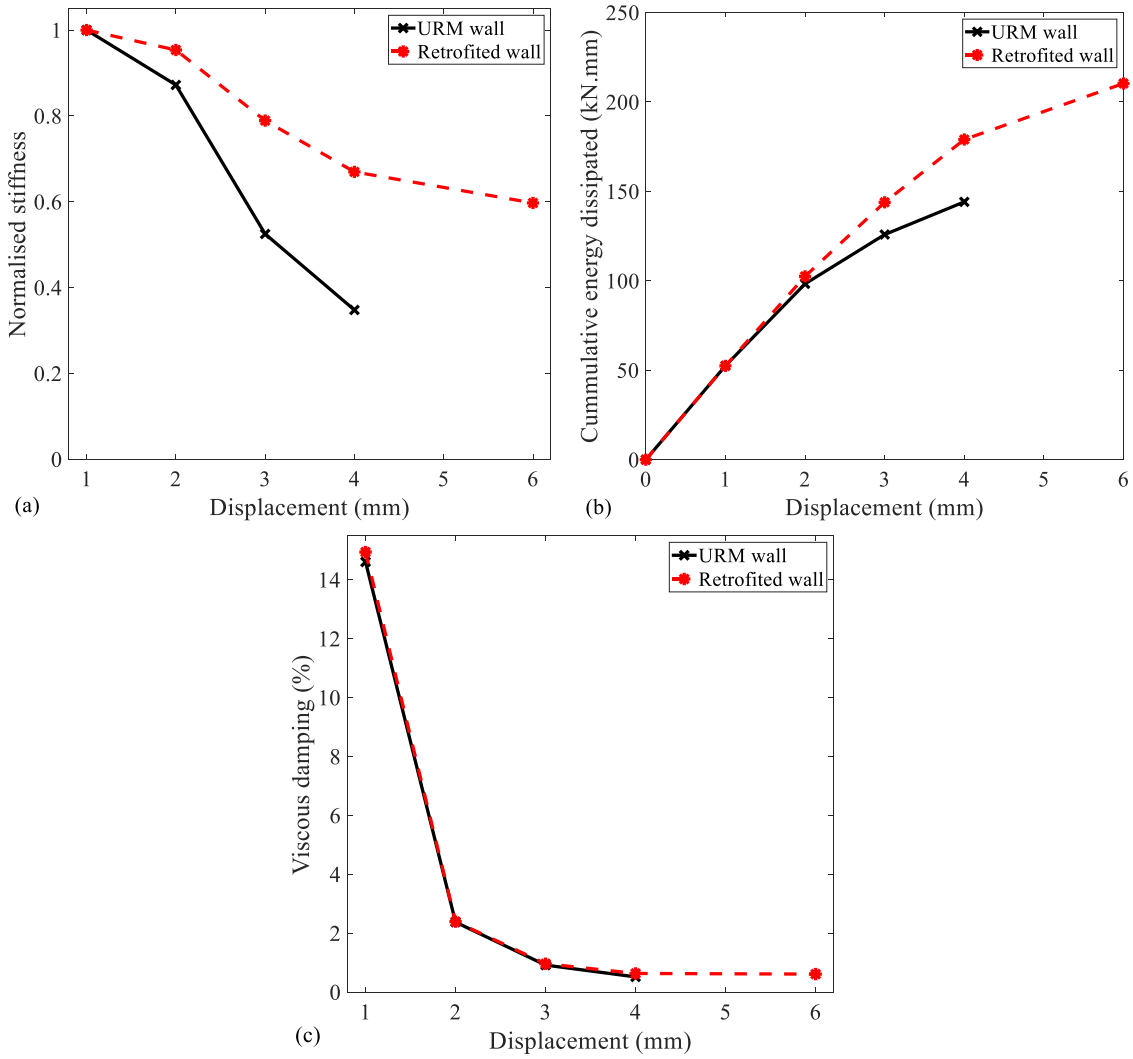

Fig. 13. The damage parameters of the URM and retrofitted walls (a) normalised effectiveness stiffness, (b) cumulative energy dissipated and (c) viscous damping.

displacement. After that, the stiffness degradation continues with repeated loading cycles.

2. The retrofitted wall increased the lateral in-plane load-carrying capacity of the masonry wall by about 91% of the URM wall. The structural ductility was also enhanced as the retrofitted wall could sustain a drift of about 15 mm and a higher load with minimal damage than the load supported at 4 mm by the URM wall. Furthermore, shear capacity is significantly improved in the retrofitted wall, as observed in the pattern of the crack damage formed.
3. Retrofitting the URM wall with the splints and bandages technique also improved the cracking pattern by reducing the crack damage from a Grade 2, as per EMS-98, with shear cracks (horizontal and diagonal) in the mortar bed of the URM to a Grade 1 (EMS scale) [83] with minimal damage having mostly hairline cracks with little spalling of the mortar cover.
4. The proposed retrofitting technique is thus very effective in increasing the lateral strength, effective stiffness, and ductility, and hence increasing the seismic resistance of substandard masonry walls in less developed countries. Moreover, the technique could also be applied to enhance the seismic performance of new and existing masonry structures in seismic-prone regions.
5. Overall, the experiment quantified the efficiency of a practical, low-cost retrofitting technique that is used worldwide and in agreement with the retrofit guidelines proposed by NSET-Nepal, thus helping build confidence in the local stakeholders and improving the reliability of the fragility models used for risk assessment.
6. The retrofitting method is recommended for application in Nepal school buildings as designed by NSET-Nepal and more in general for URM structures in less developed countries exposed to seismic hazards.

Declaration of competing interest

The authors declare that they have no known competing financial interests or personal relationships that could have appeared to influence the work reported in this paper.

Data availability

Data will be made available on request.

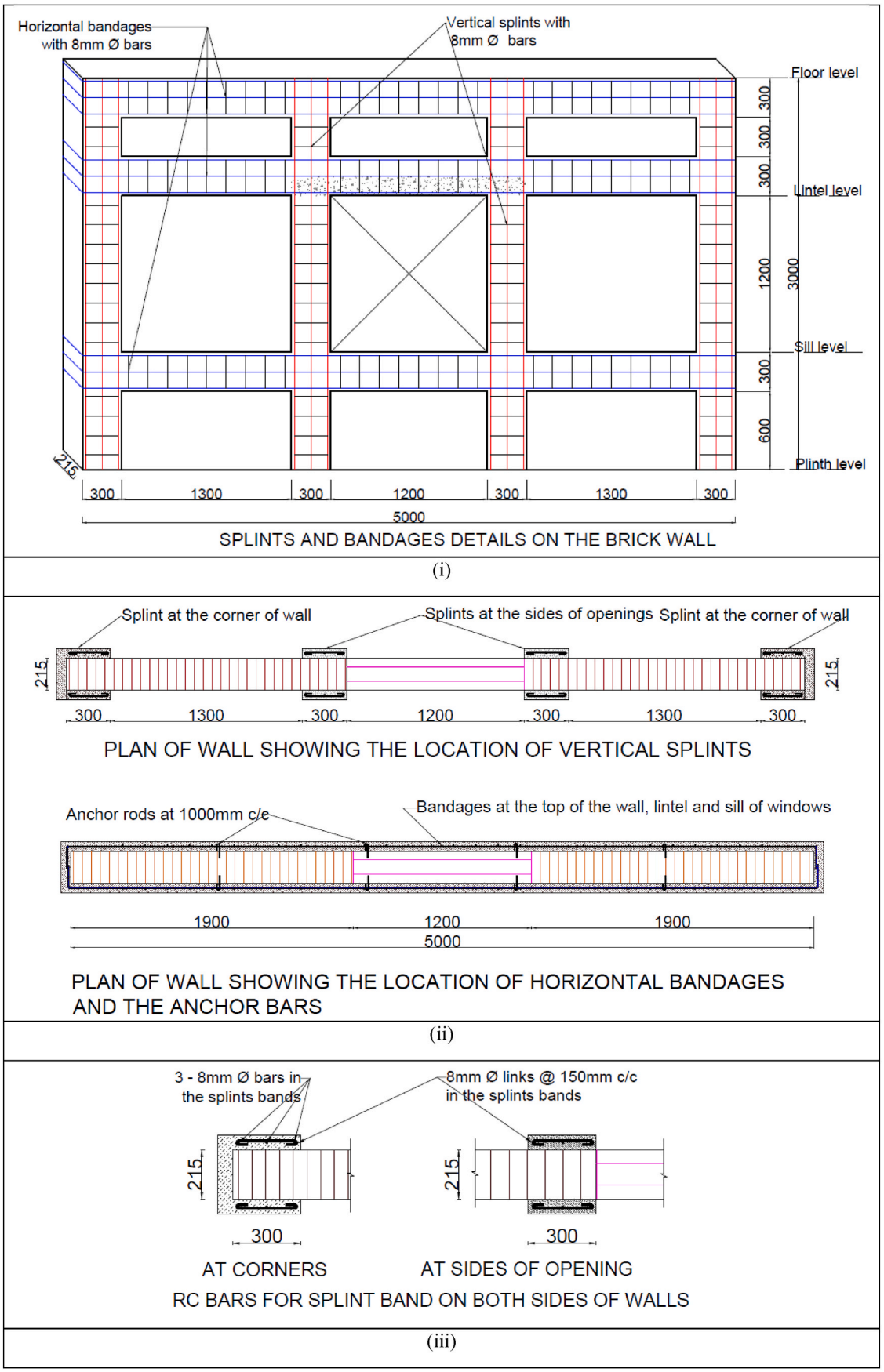

Fig. 14. The procedure for retrofitting Nepalese school buildings.

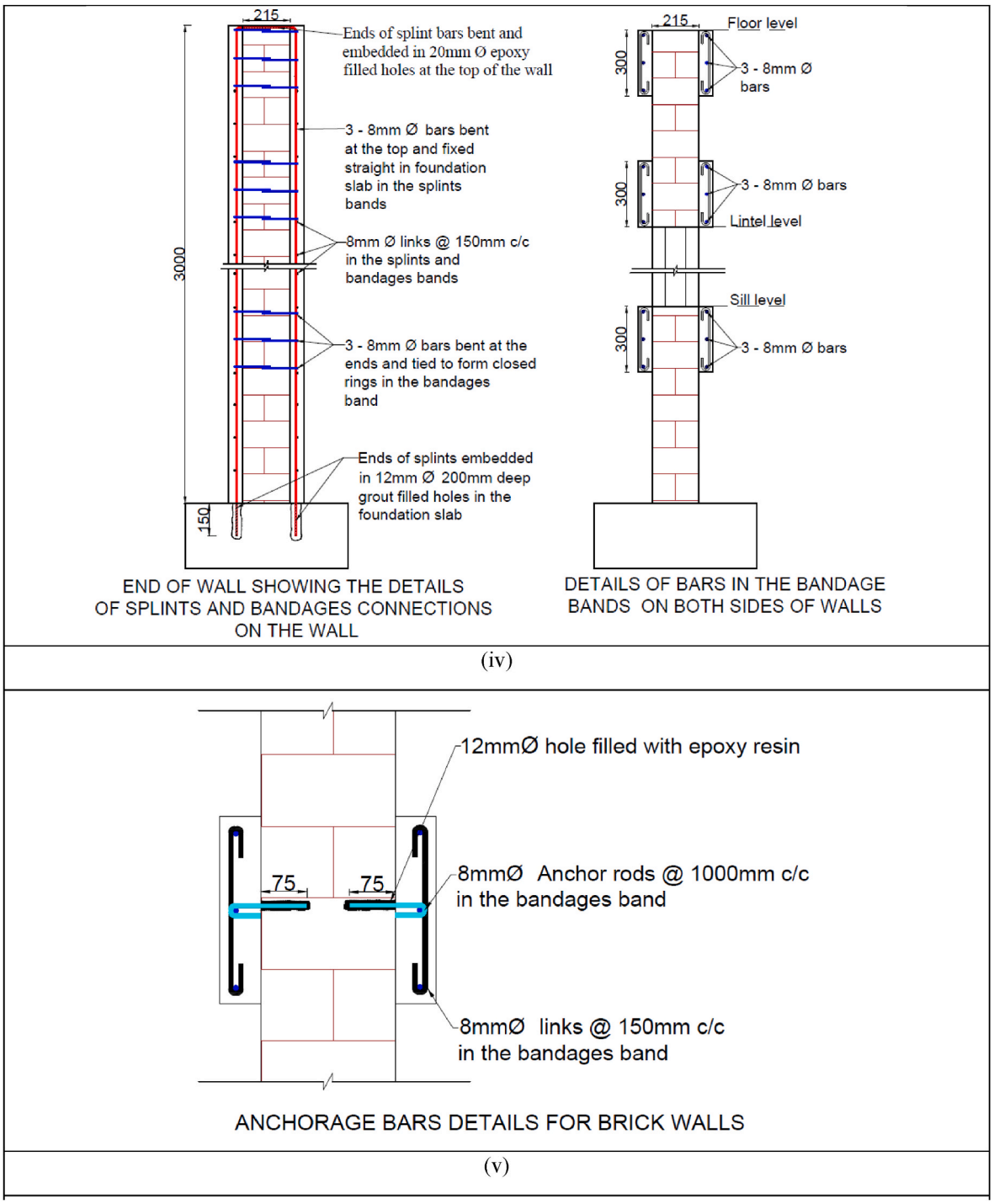

Fig. 14. (*continued*).

Acknowledgements

This work was funded by the UK Engineering and Physical Science Research Council (EPSRC) under the project "Seismic Safety and Resilience of Schools in Nepal" SAFER (EP/P028926/1). The authors acknowledged the support of the National Society for Earthquake Technology-Nepal (NSET) for the provision of models for experimental testing. We are also grateful to the technical staff at LSTL and TSRL at the University of Southampton for their assistance on the experimental test while thanking LST Projects for helping build the wall.

References

[1] Bothara JK, Dhakal RP, Mander JB. Seismic performance of an unreinforced masonry building: an experimental investigation. Earthq Eng Struct Dynam 2010; 39:45–68.
[2] Giordano N, et al. Financial assessment of incremental seismic retrofitting of Nepali stone-masonry buildings. Int J Disaster Risk Reduc 2021;60:102297.
[3] Cuadra CH, Tokeshi K. Lessons learned from the 2007 Pisco Earthquake (Peru) and recommendations for disaster mitigation. In: The 14th world conference on earthquake engineering (14WCEE); 2008 [Beijing, China].
[4] Manandhar V, et al. Experimental investigation of low cost steel wire mesh retrofit for stone masonry in mud mortar. In: 17th world conference on earthquake engineering, 17WCEE; 2020 [Sendai, Japan].

[5] Roeslin S, Ma QTM, García HJ. Damage assessment on buildings following the 19th september 2017 puebla, Mexico earthquake. Frontiers in Built Environment 2018;4 (72).
[6] Ferreira S, Karali B. Do earthquakes shake stock markets? PLoS One 2015;10(7): 1–19.
[7] Meroni F, et al. A damage scenario for the 2012 northern Italy earthquakes and estimation of the economic losses to residential buildings. Int J Disaster Risk Sci 2017;8:326–41.
[8] Aktas YD, et al. Traditional structures in Turkey and Greece in 30 october 2020 Aegean Sea earthquake: field observations and empirical fragility assessment. Frontiers in Built Environment 2022;8:1–17. 840159.
[9] Bilham R, Bodin P, Jackson M. Entertaining a great earthquake in western Nepal: historic inactivity and geodetic tests for the present state of strain. J Nepal Geol Soc 1995;11(1):73–8.
[10] Dizhur D, et al. Building typologies and failure modes observed in the 2015 Gorkha (Nepal) earthquake. Bull N Z Soc Earthq Eng 2016;49(2):211–32.
[11] Giordano N, De Luca F, Sextos A. Out-of-plane closed-form solution for the seismic assessment of unreinforced masonry schools in Nepal. Engineering Structures; 2020. p. 203. 109548.
[12] Paci-Green R, Pandey B, Friedman R. Safer schools, resilience communities: a comparative assessment of school safety after the 2015 Nepal earthquakes. 2015.
[13] Giordano N, De Luca F, Sextos A, Ramirez Cortes F, Fonseca Ferreira C, Wu J. Empirical seismic fragility models for Nepalese school buildings. Natural hazards 2021;105:339–62.
[14] Gautam D, et al. Common structural and construction deficiencies of Nepalese buildings. Innov. Infrastruct. Solut. 2016;1(1):1–18.
[15] Brando G, et al. Damage reconnaissance of unreinforced masonry bearing wall buildings after the 2015 Gorkha, Nepal, earthquake. Earthq Spectra 2017;33(1): 243–73.
[16] Vicente R, et al. In: Costa A, Guedes JM, Varum H, editors. *Seismic Vulnerability and risk Assessment of historic masonry buildings*. Structural rehabilitation of old buildings. Netherlands: Springer; 2014.
[17] Gautam D, Chaulagain H. Structural performance and associated lessons to be learned from world earthquakes in Nepal after 25 April 2015 (MW 7.8) Gorkha earthquake. Eng Fail Anal 2016;68:222–43.
[18] Sharma K, Deng L, Noguez CC. Field investigation on the performance of building structures during the April 25, 2015, Gorkha earthquake in Nepal. Eng Struct 2016; 121:61–74.
[19] Dong K, et al. Experimental study on seismic behavior of masonry walls strengthened by reinforced mortar cross strips. Sustainability 2019;11(4866):1–19.
[20] Tomazevic M, Lutman M. Heritage masonry buildings in urban settlements and the requirements of eurocodes: the experience of Slovenia. Int J Architect Herit 2007; 1:108–30.
[21] Vemuri JP, Kolluru S. Seismic analysis of unreinforced masonry walls. Journal of Integrated Disaster Risk Management 2016;6(2):102–15.
[22] Bhattacharya S, Nayak S, Dutta SC. A critical review of retrofitting methods for unreinforced masonry structures. Int J Disaster Risk Reduc 2014;7:51–67.
[23] Chuang SW, Zhuge Y. Seismic retrofitting of unreinforced masonry buildings – a literature review. Aust J Struct Eng 2005;6(1):25–36.
[24] Wang C, Sarhosis V, Nikitas N. Strengthening/retrofitting techniques on unreinforced masonry structure/element subjected to seismic loads: a literature review. Open Construct Build Technol J 2018;12:251–68.
[25] Yavartanoo F, Kang TH-K. Retrofitting of unreinforced masonry structures and considerations for heritage-sensitive constructions. J Build Eng 2022.
[26] Gkournelos PD, Triantafillou TC, Bournas DA. Seismic upgrading of existing masonry structures: a state-of-the-art review. Soil Dynam Earthq Eng 2022;161: 107428.
[27] Chiozzi A, Simoni M, Tralli A. Base isolation of heavy non-structural monolithic objects at the top of a masonry monumental construction. Mater Struct 2016;49: 2113–30.
[28] De Luca A, et al. Base isolation for retro+tting historic buildings: evaluation of seismic performance through experimental investigation. Earthq Eng Struct Dynam 2001;30:1125–45.
[29] Kilar V, Petrovcic S. Seismic rehabilitation of masonry heritage structures with base-isolation and with selected contemporary strengthening measures. Int. J. of Safety and Security Eng. 2017;7(4):475–85.
[30] Tomaževic M, Klemenc I, Weiss P. Seismic upgrading of old masonry buildings by seismic isolation and CFRP laminates: a shaking-table study of reduced scale models. Bull Earthq Eng 2008.
[31] Losanno D, et al. Seismic performance of a Low-Cost base isolation system for unreinforced brick Masonry buildings in developing countries. Soil Dynam Earthq Eng 2021;141:106501.
[32] Augenti N, Nanni A, Parisi F. Construction failures and innovative retrofitting. Buildings 2013;3:100–21.
[33] Benedetti A, Landi L, Merenda DG. Displacement-based design of an energy dissipating system for seismic upgrading of existing masonry structures. J Earthq Eng 2014;18(4):477–501.
[34] ElGawady MA, Lestuzzi P, Badoux M. Retrofitting of masonry walls using shotcrete. In: New Zealand society for earthquake engineering; 2006 [New Zealand].
[35] Karantoni FV, Fardis MN. Effectiveness of seismic strengthening techniques for masonry buildings. J Struct Eng 1992;118(7):1884–902.
[36] Shabdin M, Attari NKA, Zargaran M. Experimental study on seismic behavior of unreinforced masonry (URM) brick walls strengthened in the boundaries with shotcrete. J Earthq Eng 2021;25(7):1381–407.
[37] Ehteshami Moeini M, et al. Cyclic performance assessment of damaged unreinforced masonry walls repaired with steel mesh reinforced shotcrete. Eng Struct 2022;253:113747.
[38] Xin R, Ma P. Experimental investigation on the in-plane seismic performance of damaged masonry walls repaired with grout-injected ferrocement overlay. Construct Build Mater 2021;282:122565.
[39] Facconi L, et al. Analytical model for the in-plane resistance of masonry walls retrofitted with steel fiber reinforced mortar coating. Eng Struct 2023;275:115232.
[40] Rai DC, Goel SC. Seismic strengthening of unreinforced masonry piers with steel elements. Earthq Spectra 1996;12(4):845–62.
[41] Soltanzadeh G, et al. Seismic retrofit of masonry wall infilled RC frames through external post-tensioning. Bull Earthq Eng 2018;16:1487–510.
[42] Taghdi M, Bruneau M, Saatcioglu M. Seismic retrofitting of low-rise masonry and concrete walls using steel strips. J Struct Eng 2000;126(9):1017–25.
[43] Hwang SH, et al. In-plane seismic performance of open masonry walls retrofitted with steel-bar truss units. Construct Build Mater 2022;320:126278.
[44] Ruiz DM, et al. Strengthening of historical earthen constructions with steel plates: full-scale test of a two-story wall subjected to in-plane lateral load. Construct Build Mater 2023;363:129877.
[45] Amiraslanzadeh R, et al. A comparative study on seismic retrofitting methods for unreinforced masonry brick walls. In: 15th world conference on earthquake engineering; 2012 [Lisboa, Portugal].
[46] Darbhanzi A, Marefat MS, Khanmohammadi M. Investigation of in-plane seismic retrofit of unreinforced masonry walls by means of vertical steel ties. Construct Build Mater 2014;52:122–9.
[47] Liu H, et al. Quasi-static loading test of confined clay brick masonry walls retrofitted with post-tensioned tendons. In: 2nd world congress on civil, structural, and environmental engineering (CSEE'17); 2017 [Barcelona, Spain].
[48] Melatti V, D'Ayala D. Methodology for the assessment and refinement of friction-based dissipative devices. Eng Struct 2021;229(111666):1–21.
[49] Alcaino P, Santa-Maria H. Experimental response of externally retrofitted masonry walls subjected to shear loading. J Compos Construct 2008;12(5):489–98.
[50] Carozzi FG, et al. Ancient masonry arches and vaults strengthened with TRM, SRG and FRP composites: experimental evaluation. Compos Struct 2018;187:466–80.
[51] Macabuag J, Guragain R, Bhattacharya S. Seismic retrofitting of non-engineered masonry in rural Nepal. Structures and Buildings 2012;165(SB6):273–86.
[52] Mahmood H, Ingham JM. Diagonal compression testing of FRP-retrofitted unreinforced clay brick masonry wallettes. J Compos Construct 2011;15(5): 810–20.
[53] Badonbok Lyngkhoi R, Warjri T, Marthong C. Use of steel wire mesh for compressive strength enhancement of AAC masonry wall. Mater Today Proc 2023.
[54] Biolzi L, et al. Diagonal compression cyclic testing of unreinforced and reinforced masonry walls. Construct Build Mater 2023;363:129839.
[55] Zamani-Ahari G, Yamaguchi K. Experimental investigation on cyclic in-plane behavior of URM walls retrofitted with AFRP. Case Stud Constr Mater 2022;17: e01558.
[56] Deng M, et al. Out-of-plane strengthening of URM walls using different fiber-reinforced materials. Construct Build Mater 2023;362:129597.
[57] Soleymani A, et al. In-plane shear strengthening of traditional unreinforced masonry walls with near surface mounted GFRP bars. Construct Build Mater 2023; 367:130362.
[58] Borri A, et al. Shear behavior of unreinforced and reinforced masonry panels subjected to in situ diagonal compression tests. Construct Build Mater 2011;25: 4403–14.
[59] Corradi M, et al. The Reticulatus method for shear strengthening of fair-faced masonry. Bull Earthq Eng 2016;14:3547–71.
[60] Fonti R, et al. Rubble masonry response under cyclic actions: experimental tests and theoretical models. Int J Magn Reson Imag 2017;2(1):30–60.
[61] Milosevic J, et al. Experimental assessment of shear strength parameters on rubble stone masonry specimens. Construct Build Mater 2013;47:1372–80.
[62] Mirra M, Gerardini A, Ravenshorst G. Application of timber-based techniques for seismic retrofit and architectural restoration of a wooden roof in a stone masonry church. Procedia Struct Integr 2023;44:1856–63.
[63] Iovane G, et al. Timber based systems for the seismic and energetic retrofit of existing structures. Procedia Struct Integr 2023;44:1870–6.
[64] National Society for Earthquake Technology - Nepal (NSET). Proposed typologies with their seismic strengthening measures for large scale experimental tests under SAFER. 2018. p. 1–22.
[65] Shadlou M, Ahmadi E, Kashani MM. Micromechanical modelling of mortar joints and brick-mortar interfaces in masonry Structures: a review of recent developments. Structures 2020;23:831–44.
[66] Giordano N, De Luca F, Sextos A. Analytical fragility curves for masonry school building portfolios in Nepal. Bull Earthq Eng 2021;19:1121–50.
[67] Giordano N, et al. Derivation of fragility curves for URM school buildings in Nepal. In: 13th international Conference on Applications of Statistics and Probability in civil engineering, ICASP13; 2019 [Seoul, South Korea].
[68] Tsiavos A, et al. Large-scale experimental investigation of a low-cost PVC 'sand-wich' (PVC-s) seismic isolation for developing countries. Earthq Spectra 2020;36 (4):1886–911.
[69] Government of Nepal. *NBC 203:2015 Guidelines for earthquake resistant building construction: low strength masonry* department of urban development and building construction (DUDBC). Kathmandu, Nepal: Ministry of Urban Development (MoUD): Bahar Mahal; 2016.
[70] Ahmadizadeh M, Shakib H. Experimental study of the in-plane behavior of confined stone masonry walls. J Struct Eng 2016;142(4015145):13.

[71] Drougkas A, et al. Analytical models to determine in-plane damage initiation and force capacity of masonry walls with openings. J Eng Mech 2021;147(4021088):13.
[72] Vasconcelos G, Lourenço PB. In-plane experimental behavior of stone masonry walls under cyclic loading. J Struct Eng 2009;135(10):9.
[73] Hasnat A, et al. In-plane cyclic response of unreinforced masonry walls retrofitted with ferrocement. Case Stud Constr Mater 2022;17:e01630.
[74] FEDERAL EMERGENCY MANAGEMENT AGENCY (FEMA). Interim testing protocols for determining the seismic performance characteristics of structural and nonstructural components. USA: California; 2007. *FEMA 461*.
[75] LaVision GmbH, *StrainMaster DIC 1.1*. 2017, LaVision GmbH: Göttingen, Germany.
[76] The British Standards. Specification for masonry units Part 1: clay masonry units. In: BS EN 771-1:2011+A1:2015. London, UK: BSI Standards Limited; 2016.
[77] The British Standards. Methods of test for masonry units, Part 1: determination of compressive strength. In: BS EN 772-1:2011+A1:2015. London UK: BSI Standards Limited; 2015.
[78] The British Standards. Methods of test for mortar for masonry, Part 11: determination of flexural and compressive strength of hardened mortar. BS EN 1015-11:2019. London, UK: BSI Standards Limited; 2019.
[79] The British Standards. Methods of test for mortar for masonry, Part 10: determination of dry bulk density of hardened mortar. BS EN 1015-10:1999. London, UK: BSI Standards Limited; 1999.
[80] The British Standards. Steel for the reinforcement of concrete — weldable reinforcing steel — bar, coil and decoiled product — specification. In: BS 4449-2005+A3-2016. London, UK: BSI Standards Limited; 2016.
[81] The British Standards. Metallic materials — tensile testing, Part 1: method of test at room temperature. In: BS EN ISO 6892-1:2019. London, UK: BSI Standards Limited; 2020.
[82] Magenes G, Calvi GM. In-plane seismic response of brick masonry walls. Earthq Eng Struct Dynam 1997;26(11):22.
[83] Grünthal G, editor. European macroseismic scale 1998 (EMS-98), *European seismological commission, sub commission on engineering seismology, working group macroseismic scales*; 1998.
[84] Yamaguchi K, et al. Classification and effects of strengthening and retrofitting techniques for unreinforced masonry structures. In: The second bilateral Iran-o-Japan seminar on seismology and earthquake engineering of historical masonry buildings. Iran: Tabriz; 2016.
[85] Warjri T, Marbaniang DF, Marthong C. In-plane behaviour of masonry walls embedding with steel welded wire mesh overlay with mortar. Journal of Structural Integrity and Maintenance 2022;7(3):177–87.
[86] Syiemiong H, Marthong C. A review on improved construction methods for clay-brick and concrete-block ordinary masonry buildings. Journal of Structural Integrity and Maintenance 2021;6(2):67–83.
[87] Paikara S, Rai D. Confining masonry using pre-cast RC element for enhanced earthquake resistance, vol. 7. 8th US National Conference on Earthquake Engineering; 2006. 2006.
[88] Ivorra S, et al. In-plane shear cyclic behavior of windowed masonry walls reinforced with textile reinforced mortars. Eng Struct 2021;226:111343.
[89] Coccia S, Di Carlo F, Imperatore S. Masonry walls retrofitted with vertical FRP rebars. Buildings 2020;10(72):1–17.